Progress In Electromagnetics Research B, Vol. 54, 185–201, 2013

MODIFIED MODEL OF SQUIRREL CAGE INDUCTION MACHINE UNDER GENERAL ROTOR MISALIGNMENT FAULT

Hamidreza Akbari*

Department of Electrical Engineering, Yazd Branch, Islamic Azad University, Yazd, Iran

Abstract—A great deal of researches have so far been conducted on the analysis of eccentricity in induction machines. However, they mostly consider radial non-uniformity and neglect non-uniformity in the axial direction, but in practice, the axial non-uniformity due to rotor misalignment faults is quite common. This paper presents a modified model of a three-phase squirrel cage induction machine under different rotor misalignment conditions. For this purpose, general expressions for air gap and mean radius of induction machine, considering axial non-uniformity, have been developed. The proposed model is able to calculate the time varying inductances versus rotor angle for three-phase squirrel cage induction machines under general rotor misalignment, including static, dynamic and mixed rotor misalignment in the frame of a single program. Simulation results were verified by the experimental ones.

1. INTRODUCTION

The model presented by Tolyiat et al. [1] has been shown to be accurate for the time domain simulation of AC motors based on the basic geometry and winding layout of stator windings and rotor loops. Contrary to the classical d-q model, this theory can take into account all of the winding magnetomotive force space harmonics. An essential part of this theory is the calculation of machine inductances. These inductances are calculated using winding function and other equations within the theory. By this approach, all space harmonics are taken into account without any restriction concerning symmetry of stator or rotor windings. Hence, this model is widely used for the analysis of

Received 18 July 2013, Accepted 28 August 2013, Scheduled 3 September 2013

* Corresponding author: Hamidreza Akbari (hamid_r_akbari@yahoo.com).

asymmetrical and fault conditions in machines, such as broken rotor bars [2, 3] and fault condition in stator windings [4]. The modified winding function approach (MWFA) [5] for nonsymmetrical air-gap is regarded as a very powerful and general approach and has been extensively used for the last 15 years. MWFA is indeed very well suited for analyzing machines with small air gaps of arbitrary shape [6].

This method has been applied to analyze static, dynamic and mixed eccentricity in induction and synchronous machines [7–12]. In [13], different geometrical models for the calculation of inductances of induction machines were evaluated, and the best approximation was recommended. A new method for the calculation of inductances of induction machine under healthy and faulty conditions, based on combined MWFA and Magnetic Equivalent Circuit (MEC), was presented in [14].

Different eccentricities in induction machines were documented previously [7, 8, 13–18]. In reality, the most probable case is the inclined air gap eccentricity or rotor misalignment fault.

The mentioned models are not able to analyze the effects produced by the axial air-gap non-uniformity in induction machines. In [19], an extension of the MWFA for the inductance calculation considering axial non-uniformity was proposed. This method was used to calculate the mutual inductance of a three-phase induction machine under static inclined eccentricity condition. Different inclined eccentricities in induction machines have been previously documented [19–22]. In these models, only static inclined eccentricity is considered. Also, to calculate the inductances, mean radius of the machine is considered to be constant. On the other hand, the air-gap length of the machine and mean radius of the air gap are approximated, and therefore the geometrical model of the machine is simplified.

This paper presents a precise model for squirrel cage induction machine under different rotor misalignment conditions. In the presented model, precise functions of mean radius and air-gap length, considering slots effects, rotor skewing and other asymmetries, are determined.

The proposed technique is used to calculate the inductances of a three-phase squirrel cage induction machine under different misalignment conditions. Effects of stator and rotor slots, rotor skewing and several rotor axial asymmetries on inductances in these conditions are shown. Calculated inductances are also used in a coupled electromagnetic model to simulate the squirrel-cage induction machine under different healthy and rotor misalignment conditions. Finally, simulation results are compared to those obtained from experiments.

2. INDUCTANCES OF INDUCTION MACHINE UNDER AXIAL NONUNIFORMITY

In order to model eccentricity in induction machine, without skew and with uniform air-gap along the rotor, we can use the MWFA used in [13]. However, for the calculation of machine inductances under rotor misalignment conditions, considering rotor skewing, slots effect and axial non-uniformity, the extended MWFA should be used [23]. Magnetomotive force (MMF) distribution in the air gap produced by a current i_a flowing in any coil a (stator or rotor windings) is as follows:

$$F_A(\varphi, z, \theta) = N_A(\varphi, z, \theta) i_A \tag{1}$$

where, $N_a(\varphi,\ z,\ \theta)$ is the winding function of winding a, φ is arbitrary angle in stator reference frame, θ is rotor angle and z is axial position. In an electrical machine, this function can be defined for each stator and rotor windings [23].

$$N(\varphi, z, \theta) = n(\varphi, z, \theta) - \frac{\int_0^{2\pi}\int_0^l r(\varphi, z, \theta) g^{-1}(\varphi, z, \theta) n(\varphi, z, \theta) dz d\varphi}{2\pi l \int_0^{2\pi}\int_0^l r(\varphi, z, \theta) g^{-1}(\varphi, z, \theta) dz d\varphi} \tag{2}$$

where, r is the mean radius function, n the turn function, l the rotor length, and g the air gap function. A differential flux through a differential area in the air gap, $r(\varphi,\ z,\ \theta_r)dzd\varphi$, can be derived as follows:

$$d\varphi = \mu_0 N_a(\varphi, z, \theta) i_a g^{-1}(\varphi, z, \theta) r(\varphi, z, \theta) dz d\varphi \tag{3}$$

Integrating the differential flux in the region covered by coil b yields:

$$\varphi_b = \mu_0 \int_{\varphi_1}^{\varphi_2} \int_{Z_1(\varphi)}^{Z_2(\varphi)} r(\varphi, z, \theta) N_a(\varphi, z, \theta) i_a g^{-1}(\varphi, z, \theta) dz d\varphi \tag{4}$$

$n_B(\varphi,\ z,\ \theta)$ is equal to the coil turns in the region ($\varphi_1 < \varphi < \varphi_2$, $z_1(\varphi) < z < z_2(\varphi)$) and zero otherwise. Therefore, the total flux linking coil b is obtained from multiplying (3) by $n_b(\varphi,\ z,\ \theta)$ and integrating it over the whole surface:

$$\lambda_b = \mu_0 \int_0^{2\pi} \int_0^l r(\varphi, z, \theta) n_b(\varphi, z, \theta) N_a(\varphi, z, \theta) i_a g^{-1}(\varphi, z, \theta) dz d\varphi \tag{5}$$

The mutual inductance between windings a and b, considering radial and axial nonuniformity, is obtained as follows [23]:

$$L_{ba}(\theta) = \frac{\lambda_b}{i_a} \tag{6}$$

$$L_{ba}(\theta) = \mu_0 \int_0^{2\pi} \int_0^{l} \frac{r(\varphi, z, \theta) n_b(\varphi, z, \theta) N_a(\varphi, z, \theta)}{g(\varphi, z, \theta)} dz d\varphi \qquad (7)$$

Equation (7) shows that the mean radius, air gap, winding and turn are functions of φ, z and θ. Therefore, this technique has capability to simulate the mechanical asymmetry and fault of stator and rotor with no restrictions about the axial and radial non-uniformity. Also, space harmonics of the windings MMF and slots harmonics are taken into account. The winding functions of the stator phases and rotor loops of the machine do not change under the non-uniformity conditions compared to the symmetrical conditions. However, the functions of air-gap length and the mean radius will change with respect to the symmetrical case.

The winding function used in this study considers the sinusoidal variation of MMF on the slots. Fig. 1 shows the turn function of stator phase A. Phase A winding is distributed in 12 slots.

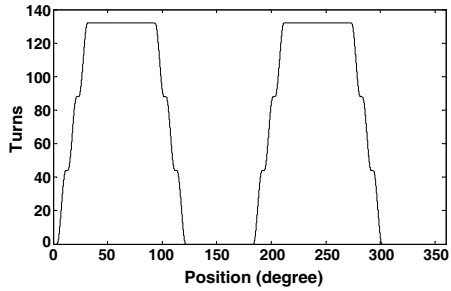

Figure 1. Turn function of the stator phase A.

3. MIXED MISALIGNMENT MODELING

The eccentricity fault occurs when the rotor axis is separated from the stator axis, while the rotor axis remains parallel to that of the stator. Eccentricity can be categorized into three general groups: Static eccentricity (SE), Dynamic eccentricity (DE) and mixed eccentricity (ME).

Rotor misalignment is caused by improper alignment of right and left bearing centers. Consequently, the centerlines of rotor shaft and stator bore are not parallel. Therefore, along the axial direction, the degree of eccentricity is not constant. To model the rotor misalignment, this fault can be treated as a variable circumferential eccentricity. Rotor misalignment fault can also be subdivided into three categories;

static misalignment (SM), dynamic misalignment (DM) and mixed misalignment (MM).

Contrary to the winding function, the air-gap function and the mean radius function change in non-uniformity conditions compared to the symmetrical case. It is intended to develop these functions which express the geometrical model of the machine.

Figure 2 shows an elementary induction machine with static rotor misalignment. In this condition, the symmetrical axis of rotor, which is superimposed to the rotor rotating axis, is inclined relative to the symmetrical axis of stator.

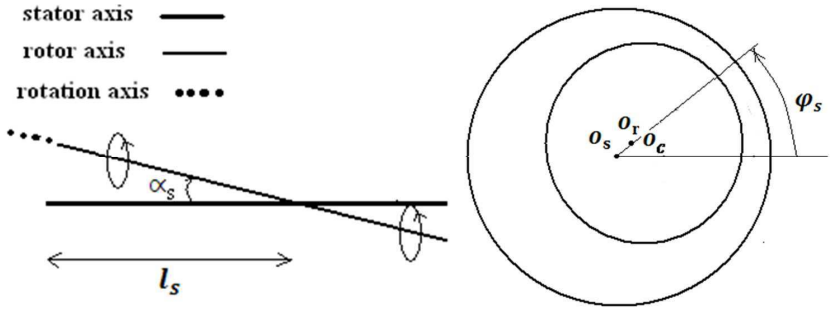

Figure 2. Static misalignment in an induction machine. (a) Axes position and (b) a cross section of machine. O_s is stator center, o_r is rotor center and O_c is rotor rotating center.

In this condition, the air gap length variation can be described by air gap function as follows:

$$g(\varphi, \theta, \varphi_s, z) = g_H(\varphi, \theta)(1 - \delta_s(z)\cos(\varphi - \varphi_s)) \tag{8}$$

where g_H is the air gap function in healthy condition, g_M the air gap function in case of rotor misalignment, φ_s the angle at which rotor rotation and stator centers are separated, and δ_s the static eccentricity level. φ_s is clearly shown in Fig. 2(b) and δ_s obtained from the ratio between the distance of stator and rotation centers ($o_s o_c$ in Fig. 2(b)) and air gap length of healthy machine. Through geometric analysis on Fig. 2(a), it is straightforward to show the static eccentricity level at any point along the axial direction as

$$\delta_s(z) = -\tan(\alpha_s)(z - l_s)/g_0 \tag{9}$$

α_s is the inclined angle of the rotor and l_s the shaft misalignment level in the case of static misalignment. α_s and l_s are clearly shown in Fig. 2(a). The variation of static air gap eccentricity coefficient versus axial position in this condition is shown in Fig. 3.

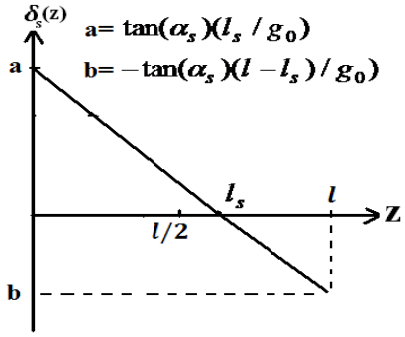

Figure 3. Variation of static eccentricity coefficient in different positions for machine under static misalignment.

The mean radius function is obtained as follows:

$$r(\varphi, \theta, \varphi_s, z) = r(\varphi) - \frac{g(\varphi, \theta, \varphi_s, z)}{2} \tag{10}$$

where, $r_s(\varphi)$ is the inner stator radius of induction machine. Mean radius function depends on the geometry of the air gap. In many studies, this function has been considered to be constant [7, 8, 13–22]. Fig. 4 shows variation of mean radius of the air gap for the healthy and faulty induction machine. The slots effects are taken into account by using the technique introduced in [24].

Dynamic misalignment is shown in Fig. 5. As shown, in this condition, the symmetrical axis of rotor is inclined relative to the stator symmetrical axis which is superimposed to the rotor rotating axis. The air gap length variation can be described by air gap function as follows:

$$g(\varphi, \theta, \varphi_d, z) = g_h(\varphi, \theta)(1 - \delta_d(z)\cos(\varphi - \varphi_d)) \tag{11}$$

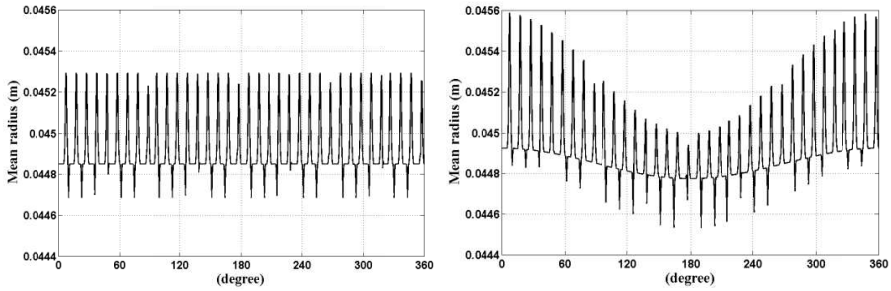

Figure 4. Mean radius function in cases of (a) healthy and (b) rotor misalignment where ($\theta = 0$, $z = 0$).

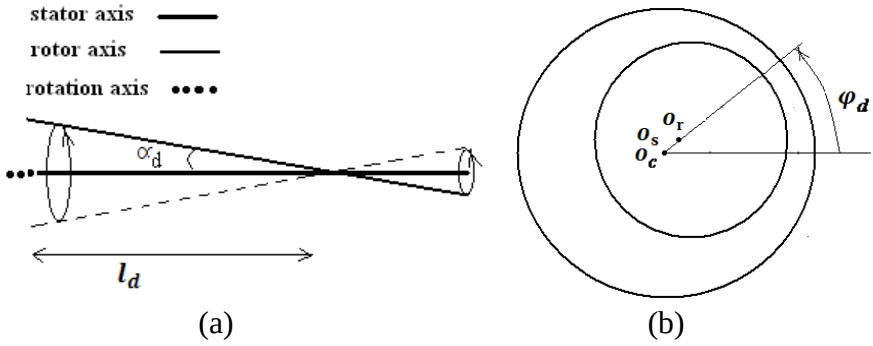

Figure 5. Dynamic misalignment in an induction machine. (a) Axes position and (b) a cross section of machine

where φ_d is angle at which rotation and rotor centers are separated, and δ_d is dynamic eccentricity coefficient. φ_d is clearly shown in Fig. 5(b). δ_d is obtained from the ratio between the distance of rotor and rotation centers (O_cO_r in Fig. 5(b)) and air gap length of healthy machine. Through geometric analysis on Fig. 5(a), it is straightforward to show the dynamic eccentricity level at any point along the axial direction as

$$\delta_d(z) = -\tan(\alpha_d)(z - l_d)/g_0 \tag{12}$$

α_d is the inclined angle of the rotor and l_d the shaft misalignment level in this case.

In reality, static and dynamic cases tend to coexist. In the case of the mixed rotor misalignment, rotor axis and rotating axis are separated from each other and are inclined compared to stator axis (Fig. 6). The air gap length variation can be described by air gap function as follows:

$$g(\varphi, \theta, \varphi_s, \varphi_d, z) = g_h(\varphi, \theta)(1 - \delta_s(z)\cos(\varphi - \varphi_s) - \delta_d(z)\cos(\varphi - \varphi_d)) \tag{13}$$

The static and dynamic cases are special cases of the mixed misalignment, where $\delta_d(z) = 0$ in static and $\delta_s(z) = 0$ in dynamic. The mean radius of the air gap is derived as (10).

The air gap function and mean radius function express the geometrical model of induction machines. The geometrical model can then be defined for induction machine with a general rotor misalignment fault including static, dynamic and mixed cases in a unified technique. So it is possible to model different types and degrees of rotor misalignments, without any restriction about axial non-uniformity.

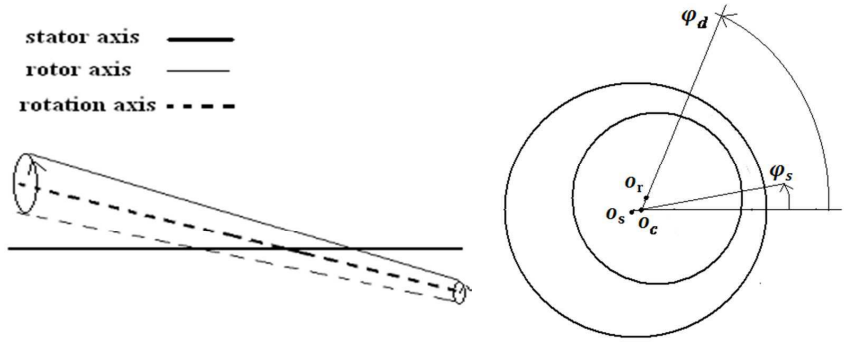

Figure 6. Mixed misalignment in an induction machine. (a) Axes position and (b) a cross section of machine.

4. SKEW EFFECT MODELING

To model the rotor skewing, the rotor is axially divided to several cross sections. The length of the air-gap and the mean radius functions are as follows:

$$g_{skew}(\varphi, z, \varphi_s, \theta) = g\left(\varphi, z, \varphi_s, \theta - \frac{\rho}{l}z\right) \tag{14}$$

$$r_{skew}(\varphi, z, \varphi_s, \theta) = r_s(\varphi) - g_{skew}\frac{g_{skew}(\varphi, z, \varphi_s, \theta)}{2} \tag{15}$$

where ρ is the mechanical angle of skewing and $g(\varphi, 0, \varphi_s, \theta)$ the air-gap function in the cross section in front of the rotor ($z = 0$). Fig. 7 shows the turn functions of the rotor loops, considering rotor skewing. The machine has 28 rotor bars on the cage.

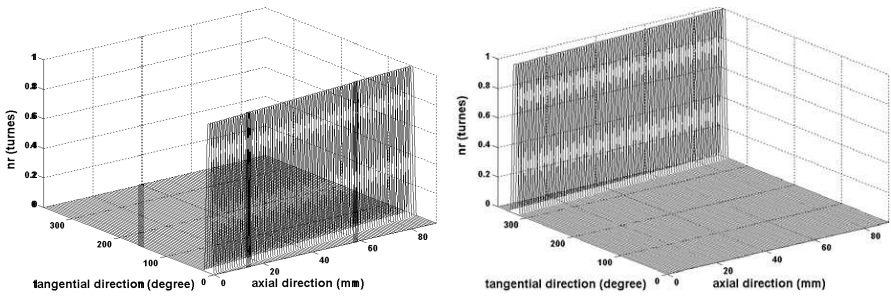

Figure 7. Turn function of (a) the rotor loop 1 and (b) rotor loop 28, considering skew effect.

5. CALCULATION OF INDUCTANCES

In this section, inductances of a 2200 W, 220 V, three-phase induction machine are calculated under different rotor misalignment conditions. Specifications of the proposed motor have been summarized in Table 1. Inductances are calculated using the Eq. (7) and presented model. All the inductances are computed at several rotor angular positions and stored within a computer file. It should be noted that the saturation and leakage flux have not been considered.

Table 1. Specifications of simulated motor.

Number of poles	4
Inner diameter of stator (mm)	90
Air gap length (mm)	0.3
Core length (mm)	90
Number of stator slots	36
Number of rotor slots	28
Rated voltage, V	380
Rated frequency, Hz	50
Rated power, hp	3

Figure 8 shows the calculated mutual inductance in thick line and its derivative in thin line. As shown in Fig. 8(b), due to skew effect, the derivative of mutual inductance between stator phases and rotor loops has lower variations. On the other hand, shape of inductance gets smooth in presence of skew.

Comparison of plots in Figs. 9 and 10 shows how SM, DM and MM affect the profile of the magnetizing inductance of stator phase A and mutual inductance between stator phase A and rotor loop 1. Eccentricity level at two ends of machine is specified on these figures. For example, In SM (SE = 20% & SE = 40%) condition, static eccentricity level at two ends of machine is 20% and 40% and in DM (DE = 60% & DE = 70%), dynamic eccentricity level at two ends of machine is 60% and 70% respectively. As shown in Fig. 9, static misalignment causes an asymmetrical mutual inductance between stator phase A and rotor loop 1 and a symmetrical magnetizing inductance of stator phase A with a larger magnitude compared to the non-eccentric condition.

As shown in these figures, in SM case, the magnetizing inductance is independent of θ, but in DM and MM cases, it is a function of the rotor angle. The reason is that in the cases of the DM and

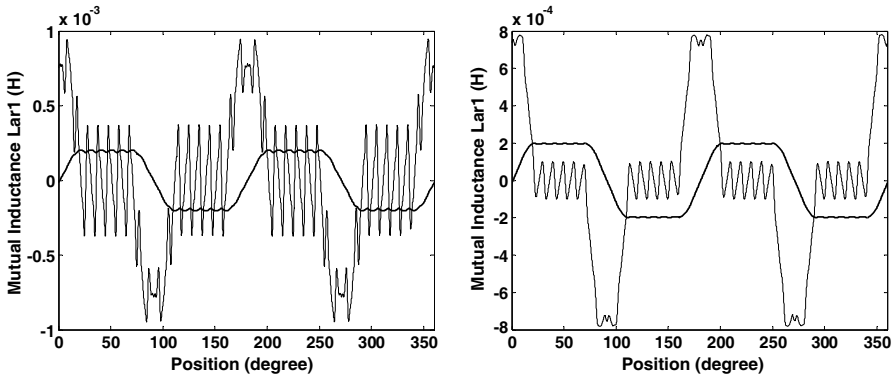

(a) (b)

Figure 8. Mutual inductance between stator phase A and rotor loop 1 (thick line) and its derivative (thin line). (a) Without skew, (b) with skew.

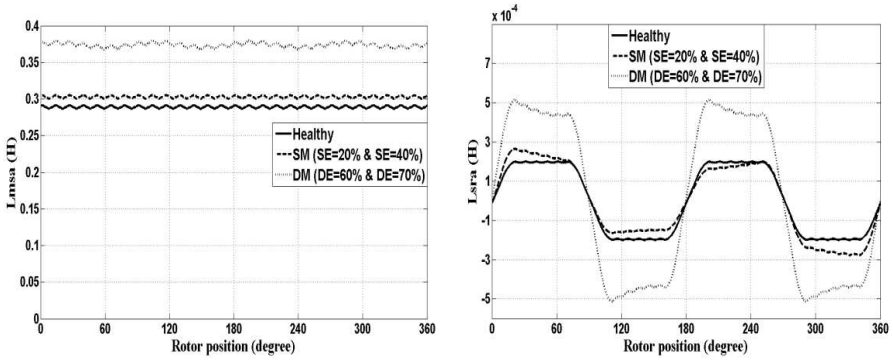

(a) (b)

Figure 9. Magnetizing inductance of (a) stator phase A and (b) mutual inductance between phase A and rotor loop 1, as a function of rotor position under healthy, static and dynamic rotor misalignment conditions.

MM, the air gap permeance is rotor position dependent. Since the rotor angular position varies continuously, the distribution of the magnetizing inductance of stator phase A is not constant. It is obvious again that by increasing the average eccentricity level, the magnitude of this inductance increases. The ripple which is present in the inductance profiles clearly exhibits the slots effect.

MM causes a pulsating magnetizing inductance, whereas, SM and DM cause a symmetrical magnetizing inductance with a larger

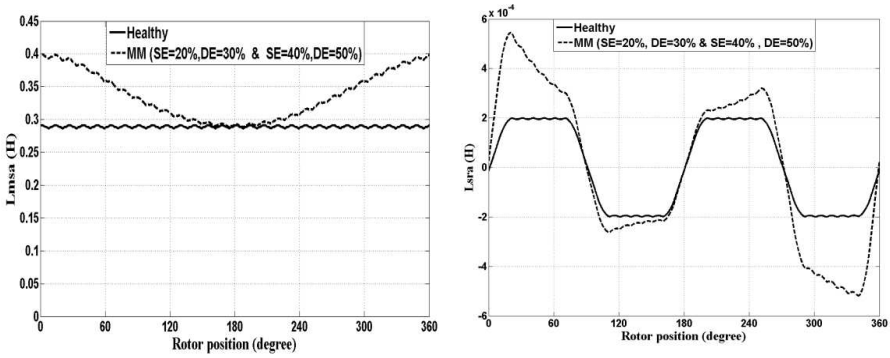

Figure 10. Magnetizing inductance of (a) stator phase A and (b) mutual inductance between stator phase A and rotor loop 1, as a function of rotor position under healthy and mixed rotor misalignment conditions.

magnitude compared to the healthy condition. SM and DM increase the magnitude of mutual inductance as such that the maximum value of mutual inductance of the healthy, 0.2 mH increases to 0.26 mH in the case of SM (one end is 20% SE and the other end is 40% SE) and to 0.51 mH in the case of DM (one end is 60% DE and the other end is 70% DE).

Referring to Fig. 10, it is seen that MM increases the mutual inductance between stator phase a and rotor loop 1 and creates asymmetrical inductance distribution. Since in the case of the MM, the minimum and maximum air gap values vary continuously, the distribution of the inductance is asymmetrical.

6. DYNAMIC SIMULATION

The calculated inductances were used in a coupled electromagnetic model to simulate and study the performance of the machine in the presence of rotor misalignment fault. The fundamental equations of multiple coupled circuit model of the machine are defined as follows [5]:

$$\mathbf{V}_s = \frac{d\boldsymbol{\lambda}_s}{dt} + \mathbf{R}_s\mathbf{I}_s \tag{16}$$

$$\mathbf{V}_r = \frac{d\boldsymbol{\lambda}_r}{dt} + \mathbf{R}_r\mathbf{I}_r \tag{17}$$

$$T_e - T_l = j\frac{dw}{dt} \tag{18}$$

$$T_e = \frac{\partial w_{co}}{\partial \theta} \tag{19}$$

where

$$w_{co} = \mathbf{I}_s^T \mathbf{L}_{ss} \mathbf{I}_s + \mathbf{I}_l^s \mathbf{L}_{sr} \mathbf{I}_r + \mathbf{I}_T^r \mathbf{L}_{rs} \mathbf{I}_s \tag{20}$$

where, $\boldsymbol{V}$ is the voltage of windings, $\boldsymbol{I}$ the current of windings, $\boldsymbol{\lambda}$ the flux linkage of windings, T_e the developed electromagnetic torque, T_1 the load torque, w_{co} the co-energy, and j the inertia of the rotor. The electromagnetic coupling model of the machine circuits is solved using a 4th and 5th order Runge-Kutta method. The simulation is performed with a symmetrical three-phase sinusoidal voltage source as the supply.

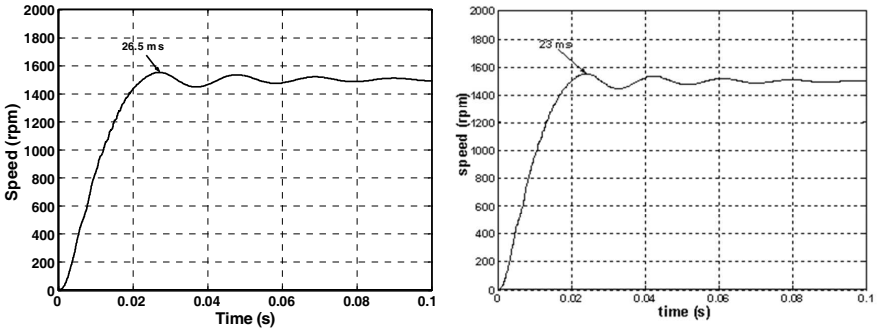

(a) (b)

Figure 11. Motor speed from (a) simulation under healthy and (b) misalignment conditions.

Figure 11 shows the motor speed from simulation under healthy and rotor misalignment conditions. As shown in the case of misalignment condition motor is started in 23 ms, where as in healthy condition motor is started in 26.5 ms. Electromagnetic motor torque depends on derivative of mutual inductances between stator phases and rotor loops. In misalignment condition, the derivative of mutual inductance has lower magnitude respect to the healthy condition. This in turn leads to increased torque magnitude in misalignment condition. Therefore, in the case of misalignment condition, motor is started faster than in the healthy condition.

7. EXPERIMENTAL RESULTS

In order to validate the simulation results, a 3-phase induction motor, similar to the simulated one, was tested under healthy and rotor

Figure 12. Test setup.

misalignment conditions. As shown in Fig. 12, tachometer was used to measure the speed. A digital oscilloscope was used to measure the induced voltage in tachometer. To be able to impose static misalignment on the rotor, a special test bed was built. The stator and the rotor bearings at the two ends of the motor were separately mounted on the test bed. This made it possible to displace any of bearings separately and create different static rotor misalignment By this manner, the induction machine with different types and degrees of static misalignment can be provided for tests.

To obtain the mutual inductance between stator phase A and phase B, a sinusoidal voltage was applied in stator phase A and the voltage induced in phase B was measured for different rotor positions from 0° to 360° taking 6° steps. The mutual inductance was calculated as follows:

$$L_{AB}(\theta) = \frac{V_B(\theta)}{V_A(\theta)} L_{AA}(\theta) \tag{21}$$

where $V_A(\theta)$ and $V_B(\theta)$ are induced voltages in stator phase A and phase B, respectively, and $L_{AA}(\theta)$ is the self inductance of stator phase A, previously calculated by means of phase A voltage and current measurements. To avoid the magnetic saturation in the experiments, a low ac voltage was applied.

Figure 13 shows the mutual inductance between stator phase A and phase B under healthy and misalignment conditions for the experiment and simulation. The experimentally obtained inductances profiles are very similar to those obtained using the proposed technique.

Figure 14 shows the motor speed from experiment under healthy and misalignment (SE = 50% & SE = 60%) conditions. As shown, the maximum speed value cannot be determined precisely due to noise. For measurement of motor speed, the experiments were repeated several times. In the case of misalignment condition, the average start time is approximately 22.3 ms, and in healthy condition, average start time is approximately 23.4 ms. The influence of misalignment on the speed

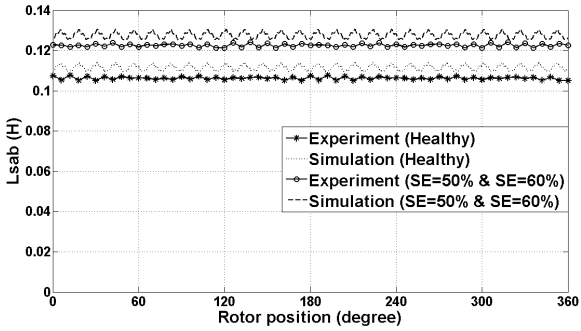

Figure 13. Mutual inductance between stator phase A and phase B under healthy and rotor misalignment (SE = 50% & SE = 60%) conditions for the experiment and simulation.

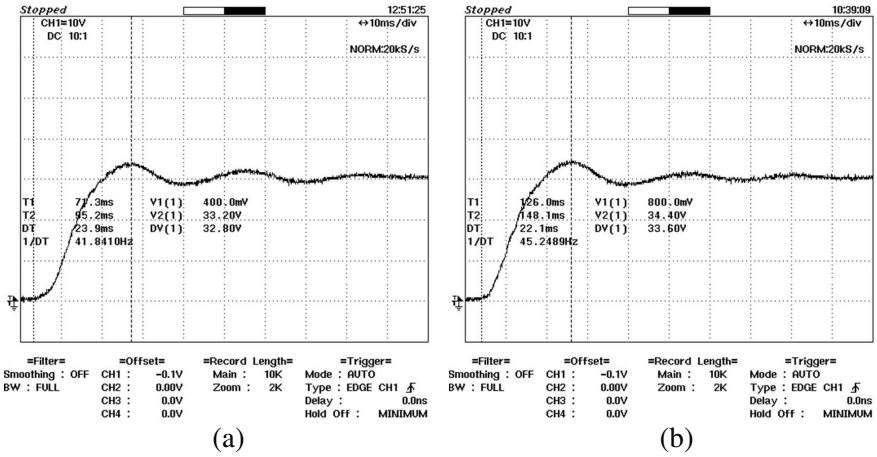

Figure 14. Motor speed from experiment under (a) healthy and (b) misalignment.

transient is relatively small. It is worth noting that the present research does not intend to derive a method to detect the misalignment fault from motor speed responses. Motor speed responses and inductance profiles from simulation and experiment are compared to verify the proposed model. Comparison between simulation and experimental results indicates a good agreement.

Probably the discrepancy between results from the proposed method and the experiments is due to neglecting the magnetic saturation. This claim needs more detailed study.

8. CONCLUSIONS

The effects of rotor misalignment fault have been previously addressed in induction motors. In these studies, only static non-uniformity is modeled, assuming that mean radius of the air gap is constant. In this paper, a more precise geometrical model of three-phase squirrel cage induction machine under different rotor misalignment conditions, considering rotor skewing, slots effect and variable mean radius function is presented. The proposed comprehensive geometrical model is able to calculate the time-varying inductances of induction machines with any rotor misalignment type and degree in a unified technique. The extended MWFA and the proposed model were used to calculate the inductances of the induction machine, under healthy and different rotor misalignment faults. Simulation results show that in the case of rotor misalignment condition, motor starts faster than in the healthy condition. Good agreement is found between the simulated and the experimental inductances profiles. Since the calculation of inductances is an essential step for simulation and analysis of fault in the machine, the proposed method can improve the on-line diagnosis of the fault.

ACKNOWLEDGMENT

This work was supported by Islamic Azad University, Yazd Branch, Yazd, Iran. The author would like to thank Dr. Homayoun Meshgin Kelk for providing information regarding the installed 2200 W induction machine in the electrical machines research Lab., Tafresh University, Iran and Prof. Jafar Milimonfared from Amirkabir University of technology, Tehran, Iran.

REFERENCES

1. Toliyat, H. A., T. A. Lipo, and J. C. White, "Analysis of a concentrated winding induction machine for adjustable speed drive applications, part-1 (motor analysis)," *IEEE Trans. on Energy Conversion*, Vol. 6, 679–692, Dec. 1991.
2. Toliyat, H. A. and T. A. Lipo, "Transient analysis of cage induction machines under stator, rotor bar and end ring faults," *IEEE Trans. on Energy Conversion*, Vol. 10, No. 2, 241–247, Jun. 1995.
3. Milimonfared, J., H. M. Kelk, A. Der Minassians, S. Nandi, and H. A. Toliyat, "A novel approach for broken bar detection in cage induction motors," *IEEE Trans. on Industry Applications*, Vol. 35, 1000–1006, Sep. 1999.

4. Joksomovic, M. G. and J. Penman, "The detection of inter turn short circuits in the stator windings of operating motors," *IEEE Trans. on Industry Application*, Vol. 47, 1078–1084, Oct. 2000.
5. Al-Nuim, N. A. and H. A. Toliyat, "A novel method for modeling dynamic air-gap eccentricity in synchronous machines based on modified winding function theory," *IEEE Trans. on Energy Conversion*, Vol. 13, 156–162, Jun. 1998.
6. Serrano-Iribarnegaray, L., P. Cruz-Romero, and A. Gomez-Exposito, "Critical review of the modified winding function theory," *Progress In Electromagnetics Research*, Vol. 133, 515–534, 2013.
7. Nandi, S., S. Ahmed, and H. A. Toliyat, "Detection of rotor slot and other eccentricity related harmonics in a three phase induction motor with different rotor cages," *IEEE Trans. on Energy Conversion*, Vol. 16, 253–260, 2001.
8. Nandi, S., R. Bharadwaj, and H. A. Toliyat, "Performance analysis of three phase induction motor under mixed eccentricity condition," *IEEE Trans. on Energy Conversion*, Vol. 17, 392–399, Sep. 2002.
9. Tabatabaei, I., J. Faiz, H. Lesani, and M. T. Nabavi-Razavi, "Modeling and simulation of a salient pole synchronous generator with dynamic eccentricity using modified winding function approach," *IEEE Trans. on Magnetics*, Vol. 40, No. 3, 1550–1555, May 2004.
10. Akbari, H., J. Milimonfared, and H. Meshgin Kelk, "A novel technique for the computation of inductances of salient pole machines under different eccentricity conditions," *Electric Power Components and Systems*, Vol. 39, No. 14, 1507–1522, 2011.
11. Faiz, J., B. M. Ebrahimi, M. Valavi, and H. A. Toliyat, "Mixed eccentricity fault diagnosis in salient pole synchronous generator using modified winding function method," *Progress In Electromagnetics Research B*, Vol. 11, 155–172, 2009.
12. Akbari, H., "An improved analytical model for salient pole synchronous machines under general eccentricity fault," *Progress In Electromagnetics Research B*, Vol. 49, 389–409, 2013.
13. Faiz, J., I. T. Ardekani, and H. A. Toliyat, "An evaluation of inductances of a squirrel-cage induction motor under mixed eccentric conditions," *IEEE Trans. on Energy Conversion*, Vol. 18, No. 2, 252–258, Jun. 2003.
14. Meshgin Kelk, H., J. Milimonfared, and H. A. Toliyat, "A Comprehensive method for the calculation of inductance coefficients of cage induction machines," *IEEE Trans. on Energy*

Conversion, Vol. 18, No. 2, 187–193, Jun. 2003.

15. Joksimovic, G. M., M. Durovic, J. Penman, and N. Arthur, "Dynamic simulation of dynamic eccentricity in induction machines-winding function approach," *IEEE Trans. on Energy Conversion*, Vol. 15, No. 2, 143–148, 2000.
16. Joksimovic, G., "Dynamic simulation of cage induction machine with air gap eccentricity," *IEE Proc. Electr. Power Appl.*, Vol. 152, No. 4, 803–811, 2005.
17. Faiz, J. and M. Ojaghi, "Unified winding function approach for dynamic simulation of different kinds of eccentricity faults in cage induction machines," *IET Electr. Power Appl.*, Vol. 3. No. 5, 461–470, 2009.
18. Ghoggal, A., S. E. Zouzou, M. Sahraoui, H. Derghal, and A. Hadri-Hamida, "A winding function-based model of air-gap eccentricity in saturated induction motors," *International Conference on Electrical Machines*, 2739–2745, 2012, DOI: 10.1109/ICElMach.2012.6350274.
19. Bossio, G., C. D. Angelo, J. Solsona, G. Garcia, and M. I. Valla, "A 2-D model of the induction machine: An extension of the modified winding function approach," *IEEE Trans. on Energy Conversion*, Vol. 19, No. 1, 144–150, Mar. 2004.
20. Li, X. D. and S. Nandi, "Analysis of a 3-phase induction machine with inclined static eccentricity," *IEEE International Conference on Electric Machines and Drives*, 1606–1613, 2005, DOI:10.1109/IEMDC.2005.195934.
21. Li, E. and S. Nandi, "Performance analysis of a three phase induction machine with inclined static eccentricity," *IEEE Trans. on Industry Application*, Vol. 43, No. 2, 531–541, 2007.
22. Kaikaa, M. and M. Hadjami, "Effects of the simultaneous presence of static eccentricity and broken rotor bars on the stator current of induction machine," *IEEE Trans. on Industrial Electronics*, 2013, DOI:10.1109/TIE.2013.2270216.
23. Akbari, H., H. Meshgin-Kelk, and J. Milimonfared, "Extension of winding function theory for radial and axial non-uniform air gap in salient pole synchronous machines," *Progress In Electromagnetics Research*, Vol. 114, 407–428, 2011.
24. Nandi, S., "Modeling of induction machines including stator and rotor slot effects," *IEEE Trans. on Industry Applications*, Vol. 40, No. 4, 1058–1065, 2004.